Numerically Robust Six-Equation Two-Phase Flow Model for Stationary and Moving Systems in Modelica

Johannes Brunnemann[1] Ales Vojacek[1] Thomas Koch[1]

[1]XRG Simulation GmbH, Germany, {brunnemann,vojacek,koch}@xrg-simulation.de

Abstract

We present a physics based Modelica finite volume flow model that separately balances vapour and liquid phase. By using extensive state variables and a special mass flow regularisation, the model can cope with the possible vanishing or emerging of a phase in a numerically robust way. Although at prototype stage, the model already exhibits all required capabilities. These are demonstrated in feature testers and in a model of a natural convection driven cooling cycle operating under external acceleration forces.
Keywords: two phase flow, six equation model, evaporating and cooling cycle, natural convection, moving systems, ClaRa library

1 Introduction

For the modelling of two phase flows, the assumption of a homogeneous spatial mixture of liquid and vapour phase is widely used in Modelica. Both phases are taken in thermal and mechanical equilibrium (equal temperature and static pressure) and form a lumped mass flow. However these assumptions are not always applicable, in particular in situations where vapour and liquid phase are expected to move independently. Within the NAKULEK[1] project options for passive cooling of power electronics in aircrafts have been investigated regarding their dimensioning and reliability under aircraft flight conditions. In these cooling circuits liquid coolant evaporates at the hot electronic equipment. The vapour then releases its heat in a condenser, see figure 7. The flow of the coolant is solely driven by natural convection. However sufficient heat removal has to be ensured at any time during operation of the aircraft. Hence the effect of external acceleration forces due to flight manoeuvres on the coolant flow has to be analysed, in particular rotations of the cooling circuit. These may lead to induced liquid flows, shifting vapour and liquid volume fractions at different spatial positions in the circuit. Experimental studies have been conducted by the project partners TUHH (Albertsen and Schmitz 2019) and ZAL (Quaium and Kuhn 2020), that additionally employ phase change material at the evaporator in order to buffer heat flow peaks.

Based on the ClaRa library (ClaRa Development Team 2021) a Modelica library containing supplementary system models of the test facilities was created by the project partner XRG Simulation GmbH (Brunnemann 2020).

This paper introduces a central element of that library: a detailed two phase flow model, based on a finite volume realisation of the so called 6-equation approach. It provides balance equations for mass, energy and momentum separately for vapour and liquid phase (hence 6-equation model) and considers dynamic external acceleration while allowing counter-directional movement of the phases. Although the model is at prototype stage it already exhibits all desired capabilities, as demonstrated in section 3.

2 Model Development

The 6-equation model approach is well established in the literature (Whalley 1987; Sokolichin 2003; Brennen 2005; Ghiaasiaan 2008) and realised in several power plant simulators, e.g. APROS (Hänninen and Ylijoki 2008). In Modelica, two phase flows are mostly treated as homogeneous flows with common balance equations for both phases (3-equation model) (as e.g. in (Francke 2014) or the Modelica Standard library). Sometimes these homogeneous models are extended by phenomenological models for interphase velocity difference (slip) or heat transfer and/or friction, e.g. in (Hoppe, Gottelt, and Wischhusen 2017).

An alternative treatment is the moving boundary approach (Jensen and Tummescheit 2002; Bonilla et al. 2012), where the spatial regions of single-phase and two phase are computed dynamically, but the two-phase region is still modelled as a homogeneous model.

In (Bauer 1999) a an advanced evaporator model was presented, with a common energy balance of the phases but (optional) separate momentum balance. This model already demonstrated the advantage of extended balancing, however numerical problems occurred at vanishing vapour phase.

Separate balancing of vapour and liquid phase, doubles the number of balance equations per control volume. Beside the doubling the equations, such an extension introduces a substantial number of additional flows in the balance equations, due to interaction of the co-existing phases. An overview is given in Table 1.

2.1 Limitations of Specific Quantity Approach

For realizing a 6-equation model based on finite control volumes in Modelica one has to consider that the control

[1]NAKULEK - Natural Circulation driven Cooling of Power Electronics (German: Naturumlaufkühlung für Leistungselektronik).

Table 1. Flows considered in homogeneous 3-equation flow model compared to 6-equation model. Simple doubling for both phases is denoted by "(liq+vap)", interaction between phases is denoted by "(liq↔vap)". Additional flows of the 6-equation model are marked in blue.

Flow	*3 equation*	*6 equation*
Mass flows	convective	convective (liq+vap) phase change (liq↔vap)
Enthalpy flows	convective	convective (liq+vap) phase change (liq↔vap)
Heat flows	to wall	to wall (liq+vap) interphase (liq↔vap)
Momentum flows	static p	static p (liq+vap) water level (liq+vap)
	dynamic p	dynamic p (liq+vap) phase change (liq↔vap)
	wall friction	wall friction (liq+vap) interphase slip (liq↔vap)
	gravity	gravity (liq+vap) external acceleration

volume V_ℓ and hence the volume fraction $\varepsilon_\ell = V_\ell / V_{\text{tot}}$ of a particular phase $\ell \in \{\text{liq},\text{vap}\}$ varies with time. Only the total volume $V_{\text{tot}} = V_{\text{vap}} + V_{\text{liq}}$ is constant. Moreover for single phase flow, the other phase is totally absent. For an equation based Modelica model this implies that the time evolution for states of that particular phase ℓ becomes meaningless in the limit $\varepsilon_\ell \to 0$. This issue has been addressed e.g. in (Jensen and Tummescheit 2002; Bonilla et al. 2012) where time evolution of states of the vanishing phase are mapped onto those of the other phase as dummy equation. For this mapping the form of the balance equations has to be modified: they need to be "switched over" for volume fractions close to zero but also "switched back" to the original zone physics if the volume of that zone exceeds a certain lower bound.

The ClaRa library (ClaRa Development Team 2021) features pipe models using a homogeneous 3-equation finite volume approach, where a pipe flow is discretised along flow direction into a one dimensional so called energy grid consisting of N_{cv} control volumes (energy cells). In each energy cell specific enthalpy h and static pressure p are chosen as states. Moreover flow velocity w is balanced on a staggered flow grid consisting of $N_{cv}+1$ flow cells, see Figure 1 with (for the 3-equation model assumed) unified vapour/liquid control volumes. Time evolution for pressure is derived from the mass balance via Equation 11 and Equation 12 by using the fact that $V = const$ for the homogeneous 3-equation-approach.

While the 3-equation model assumes thermal and mechanical equilibrium (equal temperatures and static pressure) as well as spatial homogeneity of the phases, the 6-equation model only assumes mechanical equilibrium (equal static pressures). From that we created (as a first attempt) a 6-equation model with state variables $h_{vap}, h_{liq}, w_{vap}, w_{liq}, p, \varepsilon_{vap}$ and tried to cope with vanishing phases according to the "switching" of (Bonilla et al. 2012). However it turned out that the according modification of the balance equations causes numerical stability issues. In particular the "switching" procedure appears to be problematic, as all balance equations are numerically coupled. Additionally the "switch back" to physical time evolution for an emerging phase turns out to be hard to define consistently. The definition of the state derivatives for $h_{vap/liq}, w_{vap/liq}$ becomes meaningless if $mass_{vap/liq} \to 0$. Moreover the volume fraction $\varepsilon_{vap/liq}$ is directly involved into computation of friction pressure loss and heat transfer through computation of contact surfaces. If ε_{vap} is a state, then numerically it may happen that $0 \leq \varepsilon \leq 1$ can be violated by numerical precision. This in turn produces numerical instabilities, e.g. diverging heat flows. A rethinking of these issues revealed the following insights:

1. It is easier to regulate flows in a conservation law than to regulate the actual form of that law.
2. In the context of vanishing masses and dynamic control volumes we should refrain from using specific quantities as states. Rather we should only balance "countable" (extensive) quantities.
3. Static Pressure p and volume fraction ε_{vap} should not be used as states.

2.2 From Specific to Absolute Quantities

Consequently we decided to base the 6-equation model on absolute quantities, rather then specific quantities. See Table 2 for a comparison. This means, that the specific quantities are not states. The time evolution of the system does not depend on the behaviour of the specific quantities. They are just used as algebraic functions in order to define the flows of enthalpy, momentum and volume as well as inputs to the media model:

$$H_{flow} = h \cdot m_{flow} \quad I_{flow} = w \cdot m_{flow} \quad V_{flow} = v \cdot m_{flow} \quad (1)$$

Table 2. Absolute and specific quantities. For completeness particle number N and particle weight M are given in order to illustrate the 'extensive' nature of the absolute quantities. For $V = const$, Equation 11 and Equation 12 can be used in order to define a time evolution for pressure instead of mass.

Quantity	*absolute*	*specific*
particle number	N	
mass	m	$M = m/N$
internal energy	U	$u = U/m$
enthalpy	H	$h = H/m$
momentum	I	$w = I/m$
volume	V	$v = V/m$

DOI 10.3384/ecp21181539

Notice that these definition are independent of time varying cross sectional area $A_{\oslash,\ell}$ or volume V_ℓ: mass and absolute quantity are independent of volume as well as the mass flow rate $m_{flow,\ell}$, which can be computed from momentum I_ℓ according to

$$m_{flow,\ell} = w_\ell \cdot \rho_\ell \cdot A_{\oslash,\ell} = \frac{I_\ell}{\delta x} \quad . \tag{2}$$

Here we have used $A_{\oslash,\ell} = \varepsilon_\ell \cdot A_\oslash$ and the fact that overall control volume $V_{\text{tot}} = A_\oslash \cdot \delta\bar{x}$ ($\delta\bar{x}$ is the discretization length of the flow grid) is constant in time.

2.3 Alternative State Selection

We will now work out the transition to new extensive state variables in detail:

$$\{p_\ell, h_\ell, w_\ell\} \rightarrow \{m_\ell, U_\ell, H_\ell, I_\ell\} \tag{3}$$

Avoidance of specific quantities introduces one more state on the right hand side. In order to avoid p, ε as states, we use absolute Enthalpy H_ℓ in addition to internal energy U_ℓ. The model will be set up on a staggered grid according to (Figure 1). Circles inside the control volumes in Figure 1 represent state locations. Small "j" denotes flow cell labels. Capital "J" denotes energy cell labels. The volume fraction ε_{vap} is variable in each control volume. Each quantity "x" naturally defined on one of the grids can be defined on the other grid by suitable interpolation. The interpolated quantity "$\bar{x}$" is marked by an overline.

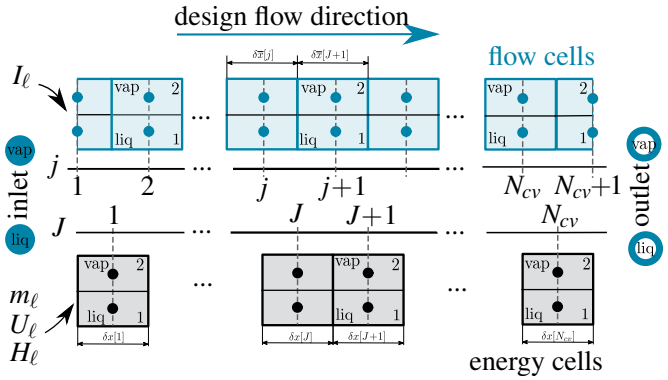

Figure 1. Staggered grid used in model with inlet and outlet connectors for each phase $\ell \in \{1,2\} \equiv \{\text{liq}, \text{vap}\}$. Top line: flow cells with momentum balance (I_ℓ). Bottom line: energy cells with mass (m_ℓ) and energy (U_ℓ, H_ℓ) balance.

We will denote the species index by ℓ, where $\ell = 1 \Leftrightarrow$ liq, $\ell = 2 \Leftrightarrow$ vap. Moreover we introduce the sign

$$\sigma_\ell = \begin{cases} 1 \text{ if } \ell = 1 \\ -1 \text{ if } \ell = 2 \end{cases}$$

With this convention we have for the total volume $V_{\text{tot}} = \text{const} = V_1 + V_2$ and define the volume fractions

$$\varepsilon_1 = \frac{V_1}{V_{\text{tot}}} = 1 - \varepsilon \qquad \varepsilon_2 = \frac{V_2}{V_{\text{tot}}} = \varepsilon \quad , \tag{4}$$

which implies

$$\frac{dV_2}{dt} = -\frac{dV_1}{dt} = V_{\text{tot}} \frac{d\varepsilon}{dt} \tag{5}$$

We assume mechanical equilibrium between the phases:

$$p = p_1 = p_2 \qquad \frac{dp}{dt} = \frac{dp_1}{dt} = \frac{dp_2}{dt} \tag{6}$$

2.3.1 Mass Balance

It is straight forward to show for the mass m_ℓ:

$$\begin{aligned} \frac{d}{dt} m_\ell[J] &= m_{flow,\ell}[j] - m_{flow,\ell}[j+1] \\ &\quad + \sigma_\ell \, m_{flow}^{(cond)}[J] - \sigma_\ell \, m_{flow}^{(evap)}[J] \end{aligned} \tag{7}$$

Mass flows $m_{flow,\ell}[j]$ are computed from momentum I_ℓ according to Equation 44. The phase change mass flows $m_{flow}^{(cond)}, m_{flow}^{(evap)}$ are computed according to section 2.6.3.

2.3.2 Energy Balance

For the internal energy U_ℓ we have:

$$\begin{aligned} \frac{d}{dt} U_\ell[J] &= H_{flow,\ell}[j] - H_{flow,\ell}[j+1] \\ &\quad + Q_{flow}^{(\ell \rightarrow int)}[J] + Q_{flow}^{(\ell \rightarrow wall)}[J] \\ &\quad + \sigma_\ell \, H_{flow}^{(cond)}[J] - \sigma_\ell \, H_{flow}^{(evap)}[J] \\ &\quad - p[J] \, \frac{dV_\ell[J]}{dt} \end{aligned} \tag{8}$$

Note that we have neglected kinetic and potential energy. For large flow velocities of considerable masses or for flows along vertical pipes these terms can be added. The convective enthalpy flows $H_{flow,\ell}[j]$ are obtained according to Equation 40. The conductive heat flows $Q_{flow}^{(\ell \rightarrow int)}[J], Q_{flow}^{(\ell \rightarrow wall)}[J]$ are described in section 2.6.1. The enthalpy flows due to phase change are computed as

$$H_{flow}^{(cond)}[J] = m_{flow}^{(cond)}[J] \cdot h^{(bub)}[i] \tag{9}$$

$$H_{flow}^{(evap)}[J] = m_{flow}^{(evap)}[J] \cdot h^{(dew)}[i] \tag{10}$$

where $h^{(bub)}, h^{(dew)}$ denote bubble / dew specific enthalpy. This assumes that the phase change enthalpy difference $\Delta h^{(evap)} = h^{(dew)} - h^{(bub)}$, stays inside the outgoing phase: condensation heat $Q_{flow}^{(cond)} = \Delta h^{(evap)} m_{flow}^{(cond)}$ stays inside the vapour phase and conversely evaporation heat $Q_{flow}^{(evap)} = \Delta h^{(evap)} m_{flow}^{(evap)}$ is taken from the liquid phase. In this way phase change is numerically stabilized, as liquid phase is more cooled and vapour phase more heated by phase change.

The last term on the right hand side of Equation 8 denotes possible expansion work, as the control volume of each phase ℓ is variable (Skogestad 2009).

2.3.3 Enthalpy Time Evolution

In the following we will leave out the ℓ-index for simplicity, but re-introduce it at the end. From the definition of mass $m = \rho V$ it follows for the density ρ in a time-dependent control volume V:

$$\frac{d\rho}{dt} = \frac{1}{V}\left\{\frac{dm}{dt} - \rho\frac{dV}{dt}\right\} \tag{11}$$

But from $\rho = \rho(p,h)$ it also holds that

$$\begin{aligned}\frac{d\rho}{dt} &= \underbrace{\left.\frac{\partial\rho}{\partial p}\right|_h}\frac{dp}{dt} + \underbrace{\left.\frac{\partial\rho}{\partial h}\right|_p}\frac{dh}{dt} \\ &= A\ \frac{dp}{dt} + B\ \frac{dh}{dt}\end{aligned} \tag{12}$$

This can be written as:

$$\frac{dp}{dt} = \frac{1}{A}\left\{\frac{d\rho}{dt} - B\frac{dh}{dt}\right\} \tag{13}$$

From $U = H - pV$ it follows that

$$\frac{dH}{dt} = \frac{dU}{dt} + \frac{dp}{dt}V + p\frac{dV}{dt} \tag{14}$$

Moreover

$$\frac{dh}{dt} = \frac{d\left(\frac{H}{m}\right)}{dt} = \frac{1}{m}\left\{\frac{dU}{dt} + \frac{dp}{dt}V + p\frac{dV}{dt} - \frac{dm}{dt}h\right\} \tag{15}$$

Here we have used Equation 14. Now we plug Equation 11 and Equation 15 into Equation 13. After some algebraic manipulations we arrive at:

$$\frac{dp}{dt} = \frac{1}{V}\frac{1}{X}\left\{Y\frac{dm}{dt} - B\frac{dU}{dt} - Z\frac{dV}{dt}\right\}, \tag{16}$$

where we have introduced the shorthands:

$$X = \rho A + B \quad Y = \rho + Bh \quad Z = \rho^2 + Bp$$

Now we can plug this into Equation 14 in order to replace the dp/dt-term. After some manipulation this gives:

$$\frac{dH}{dt} = \rho\frac{A}{X}\frac{dU}{dt} + \frac{Y}{X}\frac{dm}{dt} - \rho\frac{W}{X}\frac{dV}{dt} \quad . \tag{17}$$

Here we have used $W = \rho - pA$.

Application to liq-vap-system Now we re-introduce the species indices and set $\ell = 1 \Leftrightarrow$ liq, $\ell = 2 \Leftrightarrow$ vap. Using Equation 16 we thus get:

$$\frac{dp_1}{dt} = \frac{1}{V_1}\frac{1}{X_1}\left\{Y_1\frac{dm_1}{dt} - B_1\frac{dU_1}{dt} - Z_1\frac{dV_1}{dt}\right\} \tag{18}$$

$$\frac{dp_2}{dt} = \frac{1}{V_2}\frac{1}{X_2}\left\{Y_2\frac{dm_2}{dt} - B_2\frac{dU_2}{dt} - Z_2\frac{dV_2}{dt}\right\} \tag{19}$$

Now we subtract Equation 19 from Equation 18. Using Equation 6 and Equation 4, Equation 5 we can express:

$$\begin{aligned}V_{\text{tot}}\frac{d\varepsilon}{dt} &= -\frac{\varepsilon_2 X_2 Y_1}{Q_{12}}\frac{dm_1}{dt} + \frac{\varepsilon_2 X_2 B_1}{Q_{12}}\frac{dU_1}{dt} \\ &\quad + \frac{\varepsilon_1 X_1 Y_2}{Q_{12}}\frac{dm_2}{dt} - \frac{\varepsilon_1 X_1 B_2}{Q_{12}}\frac{dU_2}{dt}\end{aligned} \tag{20}$$

where $Q_{12} := \varepsilon_1 X_1 Z_2 + \varepsilon_2 X_2 Z_1$. Writing out Equation 17 for both phases gives:

$$\begin{aligned}\frac{dH_1}{dt} &= \rho_1\frac{A_1}{X_1}\frac{dU_1}{dt} + \frac{Y_1}{X_1}\frac{dm_1}{dt} + \rho_1\frac{W_1}{X_1}V_{\text{tot}}\frac{d\varepsilon}{dt} \\ \frac{dH_2}{dt} &= \rho_2\frac{A_2}{X_2}\frac{dU_2}{dt} + \frac{Y_2}{X_2}\frac{dm_2}{dt} - \rho_2\frac{W_2}{X_2}V_{\text{tot}}\frac{d\varepsilon}{dt}\end{aligned}$$

Now we plug in Equation 20 in order to replace the $d\varepsilon/dt$-term and can finally write for the time derivatives of the total enthalpies :

$$\left(\tfrac{d}{dt}H_1, \tfrac{d}{dt}H_2\right) = \left(\tfrac{d}{dt}m_1, \tfrac{d}{dt}U_1, \tfrac{d}{dt}m_2, \tfrac{d}{dt}U_2\right)\ \mathfrak{A} \tag{21}$$

with the matrix $\mathfrak{A}$ given as

$$\mathfrak{A} = \begin{pmatrix} \frac{Y_1}{X_1} - \rho_1\frac{W_1}{X_1}\frac{\varepsilon_2 X_2 Y_1}{Q_{12}} & \rho_2\frac{W_2}{X_2}\frac{\varepsilon_2 X_2 Y_1}{Q_{12}} \\ \rho_1\frac{A_1}{X_1} + \rho_1\frac{W_1}{X_1}\frac{\varepsilon_2 X_2 B_1}{Q_{12}} & -\rho_2\frac{W_2}{X_2}\frac{\varepsilon_2 X_2 B_1}{Q_{12}} \\ \rho_1\frac{W_1}{X_1}\frac{\varepsilon_1 X_1 Y_2}{Q_{12}} & \frac{Y_2}{X_2} - \rho_2\frac{W_2}{X_2}\frac{\varepsilon_1 X_1 Y_2}{Q_{12}} \\ -\rho_1\frac{W_1}{X_1}\frac{\varepsilon_1 X_1 B_2}{Q_{12}} & \rho_2\frac{A_2}{X_2} + \rho_2\frac{W_2}{X_2}\frac{\varepsilon_1 X_1 B_2}{Q_{12}} \end{pmatrix}$$

2.3.4 Momentum Balance

As is the case for mass and energy balance, we use absolute momentum I_ℓ as state variable, due to the time dependence of the control volume V_ℓ. Also the cross sectional flow area $\overline{A}_{\oslash,\ell}$ varies with time. Therefore we use momentum flows denoted by I_{flow}, that is we balance forces instead of force area densities (pressure drops).

$$\begin{aligned}\frac{d}{dt}I_\ell[j] &= I^{(stat)}_{flow,\ell}[j] + I^{(grav)}_{flow,\ell}[j] - I^{(wall)}_{flow,\ell}[j] + \sigma_\ell\, I^{(int)}_{flow,\ell}[j] \\ &\quad + I^{(adv)}_{flow,\ell}[J-1] - I^{(adv)}_{flow,\ell}[J] + I^{(WL)}_{flow,\ell}[J-1] - I^{(WL)}_{flow,\ell}[J] \\ &\quad + \sigma_\ell\, I^{(cond)}_{flow,\ell}[j] - \sigma_\ell\, I^{(evap)}_{flow,\ell}[j]\end{aligned} \tag{22}$$

Static pressure force. We have

$$\frac{I^{(stat)}_{flow,\ell}[j]}{A_\oslash} = \Delta p[j]\overline{\varepsilon}_\ell[j] + \mathtt{C}_{\text{supp}}\frac{d}{dt}\left(\Delta p[j]\overline{\varepsilon}_\ell[j]\right)\frac{\tau_{\text{pass}}[j]}{2} \tag{23}$$

where $\Delta p[j] = (p[J-1] - p[J])$ is the static pressure difference. $A_\oslash$ denotes the overall cross sectional area of the pipe. The second term on the right hand side can be activated via $\mathtt{C}_{\text{supp}} \in \{0,1\}$ in order to suppress numerical high frequency oscillations with $\tau_{\text{pass}}[j] = \delta\overline{x}[j]/w_{\text{sound}}[j]$ the passing time of a sound wave through the length $\delta\overline{x}[j]$ flow control volume $V[j]$.

DOI 10.3384/ecp21181539

Force due to gravity and external acceleration. The model considers acceleration $\vec{g}_{grav}$ due to gravity as well as dynamic external accelerations $\vec{g}_{ext}$ due to movement of the pipe. The resulting overall acceleration vector $\vec{g}$ is given by $\vec{g} = \vec{g}_{grav} + \vec{g}_{ext}$. Now consider the unit vetor $\vec{e}_x$ pointing into design flow direction of the pipe. It is given by $\vec{e}_x = (\vec{r}_{out} - \vec{r}_{in})/|\vec{r}_{out} - \vec{r}_{in}|$, where $\vec{r}_{out}, \vec{r}_{in}$ are the position vectors of the outlet, inlet frame connector (see section 2.7). Now we can decompose $\vec{g}$ into

$$\vec{g} = \vec{g}_{\parallel} + \vec{g}_{\perp} \tag{24}$$

where $\vec{g}_{\parallel} = \langle \vec{g}, \vec{e}_x \rangle \vec{e}_x$, $\langle \cdot, \cdot \rangle$ denotes the scalar product. Using $g_{\parallel} = |\vec{g}_{\parallel}|$ we can write for the overall force $I^{(grav)}_{flow,\ell}[j]$ induced by gravity and acceleration:

$$I^{(grav)}_{flow,\ell}[j] = g_{\parallel} \ \overline{m}_{\ell}[j] \tag{25}$$

The remainder $\vec{g}_{\perp}$ in Equation 24 is perpendicular to design flow direction and is given by $\vec{g}_{\perp} = \vec{g} - \vec{g}_{\parallel}$.

Water level force. Using $g_{\perp} = |\vec{g}_{\perp}|$ of Equation 24, we can write

$$I^{(WL)}_{flow,\ell}[J] = \frac{m_{\ell}[J]}{\delta x[J]} \ \mathtt{WL}_{\ell}[J] \ g_{\perp} \tag{26}$$

`WL` is the water level height, computed from the spatial separation model (see section 2.6.4). At clear spatial separation of the phases, `WL` causes 'acceleration' pressure $p^{(acc)}_{\ell} = \rho_{\ell} \cdot g_{\perp} \cdot \mathtt{WL}_{\ell}$ (mostly) inside the liquid. This causes an effective static pressure $p^{(eff)}_{stat,\ell} = p_{stat} + p^{(acc)}_{\ell}$. Since static pressure acts isotropically, this in turn results in $I^{(WL)}_{flow,\ell}$ along flow direction (compare to Equation 23). Here we use $\rho_{\ell} = \frac{m_{\ell}}{V_{\ell}} = \frac{m_{\ell}}{\delta x A_{\oslash} \varepsilon_{\ell}}$. Multiplying $p^{(acc)}_{\ell}$ by the phase cross sectional area $A_{\oslash}\varepsilon_{\ell}$ Equation 26 is obtained.

Wall Friction and Interphase Friction. are denoted by $I^{(wall)}_{flow,\ell}[j]$ and $I^{(int)}_{flow,\ell}[j]$, see section 2.6.2.

Force due to advection (dynamic pressure). Based on the usual formulation of the advective force,

$$I^{(adv)}_{flow,\ell} = w_{\ell} \frac{I_{\ell}}{\delta x} = w^2_{\ell} \cdot \rho_{\ell} \cdot A_{\oslash,\ell} \ , \tag{27}$$

and seeing how the mass flow and flow velocity are computed from the momentum state (Equation 2), we may write:

$$I^{(adv)}_{flow,\ell}[J] = \begin{cases} w_{\ell}[j] m_{flow,\ell}[j] & \text{if } \overline{w}_{\ell}[J] > 0 \\ w_{\ell}[j+1] m_{flow,\ell}[j+1] & else \end{cases} \tag{28}$$

In this formulation we avoid the time varying cross sectional area and density.

Phase Change Forces Beside mass and enthalpy transfer, phase change also causes momentum transfer between the phases.

$$I^{(evap)}_{flow,\ell}[j] = \overline{m}^{(evap)}_{flow}[j] \ w_1[j] \tag{29}$$

$$I^{(cond)}_{flow,\ell}[j] = \overline{m}^{(cond)}_{flow}[j] \ w_2[j] \tag{30}$$

Here the interpolated phase change mass flows are computed according to Equation 45.

2.4 Regularization of the Media Data in Case of a Vanishing Phase

We consider two VLE-media, one for the vapor phase and one for the liquid phase, that take pressure p and specific enthalpy p as inputs. Moreover we use a VLE-object taking the overall homogeneous specific enthalpy

$$h_{\text{hom}} = \frac{H_1 + H_2}{m_1 + m_2}$$

Due to the mechanical equilibrium assumption $p = p_1 = p_2$ it holds for bubble specific enthalpy that $h^{(\text{bub})}_1 = h^{(\text{bub})}_2 = h^{(\text{bub})}_{\text{hom}} = h^{(\text{bub})}$ and for dew specific enthalpy $h^{(\text{dew})}_1 = h^{(\text{dew})}_2 = h^{(\text{dew})}_{\text{hom}} = h^{(\text{dew})}$. We use the actual specify enthalpy

$$h_{\ell} = \frac{H_{\ell}}{\max(m_{reg}, m_{\ell})} \tag{31}$$

as auxiliary quantity in order to define the regularized specific quantities

$$\begin{aligned} h^{(reg)}_1 &= \min\left(h^{(bub)}, h_1\right) \\ h^{(reg)}_2 &= \max\left(h^{(dew)}, h_2\right) \end{aligned} \tag{32}$$

Here we have introduced a regulator m_{reg} for vanishing phase. The thus defined specific enthalpies $h^{(reg)}_1, h^{(reg)}_2$ are taken as input to the VLE-media objects together with static pressure p. Note that Equation 32 allows for a short time that specific enthalpy h_{ℓ} of a phase ℓ enters two phase region. However due to evaporation and condensations mass flows of Equation 54 the phase will return to pure phase after a while. The suggested construction avoids numerical issues due to heavily varying media data inside two-phase-region.

2.4.1 Pressure and Volume Fraction

The introduction of the new state variables now allows to define static pressure p and volume fraction ε_{ℓ} in terms of the new states. For $\ell = \{1,2\} = \{liq, vap\}$ we introduce the overall enthalpy $H_{\text{tot}} = H_1 + H_2$ and the total inner energy $U_{\text{tot}} = U_1 + U_2$ as well as the volume fraction $\varepsilon_1 = \varepsilon_{liq} = 1 - \varepsilon$, $\varepsilon_{vap} = \varepsilon_2 = \varepsilon$. Now we use the definitions $H_{\ell} = U_{\ell} + pV_{\ell}$ and $H_{\text{tot}} = U_{\text{tot}} + pV_{\text{tot}}$ and Equation 6 in order to write down

$$p = \frac{H_{\text{tot}} - U_{\text{tot}}}{V_{\text{tot}}} \qquad \varepsilon_{\ell} = \frac{H_{\ell} - U_{\ell}}{H_{\text{tot}} - U_{\text{tot}}} \tag{33}$$

In turn this also allows to express the time derivatives

$$\frac{d}{dt} p = \frac{1}{V_{\text{tot}}} \left(\frac{d}{dt} H_{\text{tot}} - \frac{d}{dt} U_{\text{tot}} \right) \tag{34}$$

Differentiating ε_{ℓ} with respect to time and simplifying the obtained expressions one gets for the time derivative of the volume fraction:

$$-\frac{d}{dt}\varepsilon_1 = \frac{d}{dt}\varepsilon_2 = \frac{1}{V_{\text{tot}}} \cdot \frac{\varepsilon_1 X_1 R_2 - \varepsilon_2 X_2 R_1}{Q^{(reg)}_{12}} \ , \tag{35}$$

where $R_\ell = Y_\ell \frac{dm_\ell}{dt} - B_\ell \frac{dU_\ell}{dt}$ and

$$Q_{12}^{(reg)} = \begin{cases} \varepsilon_{reg} & \text{if } |Q12| < \varepsilon_{reg} \\ Q_{12} & \text{else} \end{cases}$$

2.5 Consistent Interpolation of Half Spaced Quantities on Staggered Grid

Here we give a brief description, how quantities defined on either energy or flow cell grid Figure 1 can be consistently defined on the other grid by interpolation.

Volume

$$\overline{V}_\ell[j] = \frac{V_\ell[J-1] + V_\ell[J]}{2} \qquad \overline{V}_{\text{tot}}[j] = \overline{V}_1[j] + \overline{V}_2[j] \quad (36)$$

Cross Sectional Area

$$\overline{A}_{\oslash,\ell}[j] = \overline{A}_\oslash[j]\ \overline{\varepsilon}_\ell[j] \qquad \overline{A}_\oslash[j] = \frac{\overline{V}_{\text{tot}}[j]}{\delta\overline{x}[j]} \quad (37)$$

Length of Volume Element

$$\delta\overline{x}[j] \quad = \quad \frac{\delta x[J-1] + \delta x[J]}{2} \quad (38)$$

Volume Fraction

$$\overline{\varepsilon}_\ell[j] = \frac{\overline{V}_\ell[j]}{\overline{V}_{\text{tot}}[j]} = \frac{V_{\text{tot}}[J-1]}{2V_{\text{tot}}[j]}\ \varepsilon_\ell[J-1] + \frac{V_{\text{tot}}[J]}{2V_{\text{tot}}[j]}\ \varepsilon_\ell[J] \quad (39)$$

Mass of Flow Cells While the previous quantities are defined in a straight forward way, the mass $m_\ell[j]$ of a flow cell needs some additional considerations. In a homogeneous 3-equation model one would choose $\overline{m}_\ell[j] = (m_\ell[J-1] + m_\ell[J])/2$. However this is not consistent with the possible vanishing of a particular phase. To see this recall Equation 2, that expresses the mass flow $m_{flow,\ell}$ in terms of the momentum I_ℓ: To see this, consider two neighbour energy cells, with $\varepsilon_2[J-1] = 0$ and $\varepsilon_2[J] > 0$. Clearly, there cannot be vapour mass flow from $[J-1] \to [J]$, as $m_2[J-1] = 0$. Only vapour mass flow in opposite direction $[J] \to [J-1]$ may occur. And the model shall account for this. If we 'count' mass as a state, then the pure mass flows carry that quantity, similarly to e.g. enthalpy flows

$$H_{flow,\ell}[j] = m_{flow,\ell}[j]\overline{h}_\ell[j] \quad , \quad (40)$$

where the mass flow carries specific enthalpy $\overline{h}[j]$. In the latter case one often uses an upstream scheme in order to define specific enthalpy $\overline{h}[j]$ at the center of a flow cell, that is

$$\overline{h}_\ell[j] = \begin{cases} h_\ell[J-1] & \text{if } m_{flow,\ell}[j] > 0 \\ h_\ell[J] & \text{if } m_{flow,\ell}[j] < 0 \end{cases} \quad (41)$$

Accordingly we may use an upstream scheme for the mass $\overline{m}_\ell[j]$ of a flow cell:

$$\overline{m}_\ell^{(up)}[j] = \varsigma_\ell^{(I)}[j] \cdot m_\ell[J-1] + \left(1 - \varsigma_\ell^{(I)}[j]\right) \cdot m_\ell[J]$$

with $\varsigma_\ell^{(I)}[j] = \text{sm}(I_{reg}, 0, I_\ell[j])$, where $\text{sm}(\cdot)$ denotes the stepSmoother function contained in `Modelica.Fluid.Dissipation.Utilities`. I_{reg} is a regulator. Then we set

$$\overline{m}_\ell[j] = \max\left(m_{reg}, \overline{m}_\ell^{(up)}[j]\right) \quad , \quad (42)$$

with m_{reg} a regulator. At present, the approach still uses absolute boundaries for the regulators. In principle, these should be scaled according to a characteristical smallest number (such as smallest length or volume) of the system. This way, the approach will be robust for varying system sizes.

Flow Velocities The flow velocities can be well defined:

$$w_\ell[j] = \max\left(-w_s[j], \min\left(w_s[j], \frac{I_\ell[j]}{m_\ell[j]}\right)\right) \quad , \quad (43)$$

where we limit the flow velocity to the speed of sound w_s in order to avoid unrealistic flow velocities in the limit of small masses m_{reg}, which may lead to unwanted frictional momentum flows. By construction our model assumes subsonic flow speeds. At energy cell flow locations we use the averaged momentum

$$\overline{w}_\ell[J] = \max\left(-w_s[J], \min\left(w_s[J], \frac{I_\ell[j] + I_\ell[j+1]}{m_\ell[J]}\right)\right)$$

Mass Flows are then written as

$$m_{flow,\ell}[j] = \varsigma_\ell^{(\overline{m})}[j] \cdot \frac{I_\ell[j]}{\delta\overline{x}[j]} \quad , \quad (44)$$

where $\varsigma_\ell^{(\overline{m})}[j] = \text{sm}\left(m_{max}, m_{min}, \overline{m}_\ell[j]\right)$ and m_{max}, m_{min} are regularization parameters. This construction ensures that outgoing mass flow of a particular phase goes to *numeric* zero if the mass of that phase inside the control volume approaches zero. In particular no mass of a phase ℓ can be extracted from a control volume with $\varepsilon_\ell = 0$. On the other side mass can be easily injected from control volumes with $\varepsilon_\ell > 0$ into control volumes with $\varepsilon_\ell = 0$. This becomes especially important in situations, where e.g. vapour is injected from the outside into a pipe entirely filled with liquid.

Phase Change Mass Flows at momentum state location are computed as the sum of the phase change mass flows of the two adjacent energy half cells:

$$\overline{m}_{flow}^{(evap)}[j] = \frac{m_{flow}^{(evap)}[J-1] + m_{flow}^{(evap)}[J]}{2} \quad (45)$$

$$\overline{m}_{flow}^{(cond)}[j] = \frac{m_{flow}^{(cond)}[J-1] + m_{flow}^{(cond)}[J]}{2} \quad (46)$$

2.6 Replaceable Models

2.6.1 Heat Transfer

For each position J we have for the heat flows:

$$Q_{flow}^{(\ell \to int)} \quad = \quad \varsigma_\ell^{(m)} \cdot \alpha_{int} \cdot A_{12} \cdot (T_{int} - T_\ell) \quad (47)$$

$$Q_{flow}^{(\ell \to wall)} \quad = \quad \varsigma_\ell^{(m)} \cdot \alpha_{\ell,wall} \cdot A_{\ell,wall} \cdot (\texttt{heat.}T - T_\ell) \quad (48)$$

DOI 10.3384/ecp21181539

Here again $\varsigma_\ell^{(m)}[J] = \mathrm{sm}(m_{max}, m_{min}, m_\ell[J])$ denotes the stepsmoother function. The mean interphase surface temperature T_{int} is computed from imposing a steady state energy balance at the phase contact surface:

$$0 = \sum_\ell Q_{flow}^{(\ell \to int)} \tag{49}$$

Similarly the heat flow for the heat port is computed as

$$\texttt{heat}[J].Q_{flow} = \sum_\ell Q_{flow}^{(\ell \to wall)}[J] \tag{50}$$

2.6.2 Momentum Transfer

Wall + interfacial friction/ heat transfer models should give truly zero momentum/heat flow at vanishing phase. As default we use a 0-equation turbulence (mixing length) approach (VERSTEEG and MALALASEKERA 1995), which describes the effect of turbulence by an effective modification of dynamic viscosity μ_ℓ:

$$\mu_\ell[j] = \overline{\mu}_\ell^{(0)}[j] \cdot (1 + \mathtt{CF}_\ell \cdot \mathrm{Re}_\ell[j]); \tag{51}$$

with Reynolds number $\mathrm{Re}_\ell[j] = |w_\ell[j]| \overline{\rho}_\ell[j] \delta\overline{x}[j] / \overline{\mu}_\ell^{(0)}[j]$ and a calibration factor $\mathtt{CF}_\ell$. Then we can write for the friction between the phases

$$I_{flow,\ell}^{(int)}[j] = \frac{(w_2[j] - w_1[j])}{\max(l_{reg}, \Delta l_{12}[j])}\, \mu_\ell[j]\, A_{12}[j] \tag{52}$$

Similarly we have for the friction force between phase ℓ and the pipe walls:

$$I_{flow,\ell}^{(wall)}[j] = \frac{w_\ell[j]}{\max(l_{reg}, \Delta l_{\ell,wall}[j])}\, \mu_\ell[j]\, A_{\ell,wall}[j] \tag{53}$$

Moreover A_{12} denotes the contact area between the phases and Δl_{12} the mean distance between the center of the phase control volumes. Similarly $A_{\ell,wall}$ denotes the contact surface area between phase ℓ and pipe wall and $\Delta l_{\ell,wall}$ denotes the mean distance between phase control volume and pipe wall. At present stage, we assume ideal phase separation to derive these quantaties, as described in subsubsection 2.6.4. A flow regime model that computes A_{12} and and Δl_{12} from an effective flow pattern (e.g., ideally separated, homogeneous mixture) will be subject to future work. Also, a more sophisticated turbulence model could be implemented. From our experience Equation 51 ensures that wall and interphase friction play together in a numerically stable way.

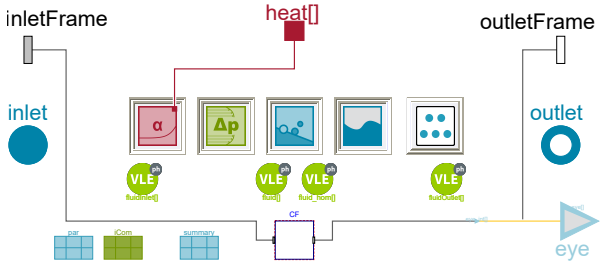

Figure 2. Diagram layer with connectors and replaceable models for heat transfer, pressure drop, phase change, spatial distribution and geometry.

2.6.3 Phase Change Models

The evaporation and condensation massflows are the massflows from the liquid to the vapour phase control volume and vice versa. They are considered to be proportional to the respective volume and, therefore, the available mass. Moreover, they scale with the steam quality and come to a halt, if the outgoing phase vanishes:

$$\begin{aligned} m_{flow}^{(evap)}[J] &= \frac{\varsigma_1^{(\varepsilon)}[J]}{\tau_{evap}} \max\left(0, \frac{h_1[J]}{h^{(bub)}[J]} - 1\right) \max\left(0, m_1[J]\right) \\ m_{flow}^{(cond)}[J] &= \frac{\varsigma_2^{(\varepsilon)}[J]}{\tau_{cond}} \max\left(0, 1 - \frac{h_2[J]}{h^{(dew)}[J]}\right) \max\left(0, m_2[J]\right) \end{aligned} \tag{54}$$

Here $\varsigma_\ell^{(\varepsilon)}[J] = \mathrm{sm}(\varepsilon_{max}, \varepsilon_{min}, \varepsilon_\ell[J])$ and $\varepsilon_{max}, \varepsilon_{min}$ are regularization parameters. Moreover we have time constants τ_{evap}, τ_{cond}. They can be thought of average time it takes for bubbles to exit from liquid to vapour phase and mean time it takes water drops coming from vapour phase in order to enter liquid phase. Larger constants mean a slower phase change mass flow, while smaller time constants would imply very dynamic phase changes. The ansatz could be improved by a flow regime depending boiling model, considering the bubble formation, mean bubble diameter and travel distance. The time constants should also be affected by the contact area of the phases.

2.6.4 Spatial Separation

This model computes certain average contact areas and distances as well as water level. So far a simple model is implemented, assuming ideal phase separation and a circular pipe cross section.

$$\begin{aligned} A_{12}[j] &= 4 \cdot \max(0, \varepsilon_1[j] \cdot \varepsilon_2[j] \cdot A_{12}^{(0)}[j]) \\ A_{\ell,wall}[j] &= \max(0, \overline{\varepsilon_\ell}[j] \cdot \overline{A}_{wall}[j]) \\ \Delta l_{12}[j] &= 4 \cdot \max(d_\oslash/100, \overline{\varepsilon}_1[j] \cdot \overline{\varepsilon}_2[j] \cdot d_\oslash/2) \\ \Delta l_{\ell,wall}[j]] &= \max(d_\oslash/100, \overline{\varepsilon}_\ell[j] \cdot d_\oslash/2) \end{aligned} \tag{55}$$

here $d_\oslash$ is the pipe diameter and $A_{12}^{(0)}[j] = \delta\overline{x}[j] \cdot d_\oslash$ is the maximum contact surface of the phases in a horizontal cylindrical pipe at ideal separation. Water level $\mathtt{WL}_1[J]$ is computed from $d_\oslash$ and liquid volume fraction $\varepsilon_1[J]$ for a horizontal cylinder volume, assuming ideal separation. Consequently $\mathtt{WL}_2[J] = d_\oslash - \mathtt{WL}_1[J]$.

2.6.5 Geometry

The model features different geometries, smilarly to ClaRa pipes, in particular it covers pipe bundles.

2.7 Connectors

Flow connectors are build from a two element array of ClaRa flow connectors `ClaRa.Basics.Interfaces.FluidPortIn` and `ClaRa.Basics.Interfaces.FluidPortOut`, one for each phase. A vanishing phase is not problematic,

since the static pressure is equal for both phases and if we ensure to have a momentum state at one side of the connector. Also in this case $h_{outflow}$ of that phase is physically not relevant and can be set to a dummy value. To connect the 6-equation model to a 3-equation component, however, one would need a suitable adapter. The adapter needs to ensure the compatibility with the flow situation: In particular a homogeneous 3-equation model cannot cope with counter flow of the phases. One `ClaRa.Basics.Interfaces.HeatPort_a` **Heat** port is attached to every control volume of the energy grid. In order to account for external acceleration each model carries **Frame** connectors from the `Modelica.Mechanics.MultiBody` package `Interfaces.Frame_a`, `Interfaces.Frame_b`. They also ensure consistency of three dimensional pipe arrangements.

3 Applications

The newly developed 6-equation model was put into feature testing (single pipe) and system testing (several pipes in system application). In this section we present three prominent examples.

3.1 Feature Tests

3.1.1 Condensation in a Tilted Pipe

This is a classic example of counter-phase flow, which is also a fair challenge for conventional CFD models: Slightly overheated steam (at 3 bars) is injected from a

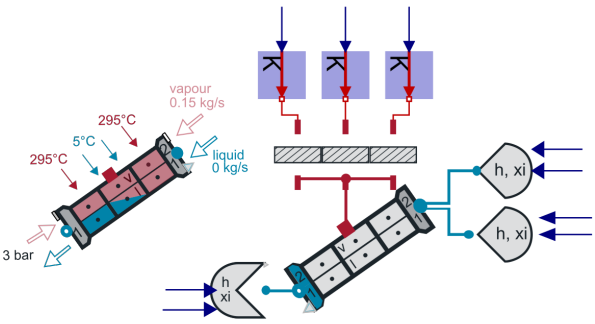

Figure 3. Condensation in the tilted pipe test model. Geometry: length L=80 m, diameter $d_{\varnothing}$=1 m, discretisation N_{CV}=40, inclination Δz=20 m.

mass flow source into an inclined pipe from the inlet. The bottom of the pipe is connected to a vapour and liquid pressure boundary condition. The first and the last 20 m of the pipe wall are heated to 295 °C. The middle section of the pipe wall (40 m) is cooled to 5 °C, such that condensation occurs. The condensed liquid flows downward in the direction of the slope. Pressure drop due to condensation causes backflow of vapour in pipe section close to the outlet. Hence, vapour is sucked into the pipe while liquid rinses out at outlet. The selected results are presented in Figure 4. The tester demonstrates applicability of the model for heat exchangers where two phase flow occurs.

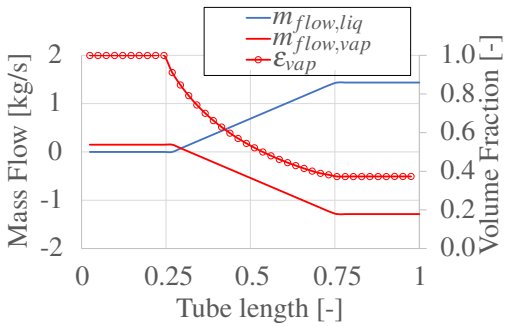

Figure 4. Resulted steady state mass flow of vapour and liquid together with volume fraction of vapour along the tilted pipe during condensation scenario.

Not only the stationary hardware, but also moving devices e.g. in vehicles, aircrafts or ships can be simulated.

3.1.2 Rotation Test

A horizontal tube is filled half with vapour and with liquid ($\varepsilon_{liq} = \varepsilon_{vap} = 0.5$). The tube is then rotated 90°downwards and back to the to the initial position. The tube is dis-

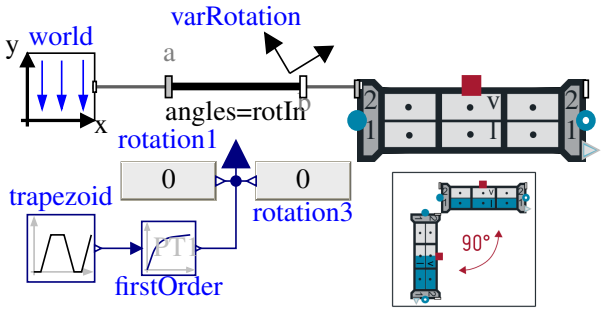

Figure 5. Rotation test model. Geometry: L=10 m, D_{in}=0.02 m, N_{CV}=41.

cretized with an odd number of control volumes. The model is shown in Figure 5. The results of the simulation scenario is presented in Figure 6 where the actual rotation angle is displayed below, and above it, the volume fraction of the liquid phase at the beginning, in the middle and at the end of the tube is shown. Before the rotation, the volume fractions are all at 50%. After the rotation, there is no more liquid at the top of the tube, while the tube end is completely filled with liquid. As expected, the volume fraction settles vertically at 50% liquid and 50% vapour. When turning back to horizontal position again, a decaying wave formation is visible (enlarged area), before the liquid level settles again uniformly at 50%.

3.2 Aircraft Cooling Circuit

3.2.1 Test Rig Model

The project partners at TUHH and ZAL (Albertsen and Schmitz 2019; Quaium and Kuhn 2020) provided detailed information on their passive cooling cycle test rigs, as well as extensive data on the conditions and results of the measurement campaigns. The basic structure of the respective

DOI 10.3384/ecp21181539

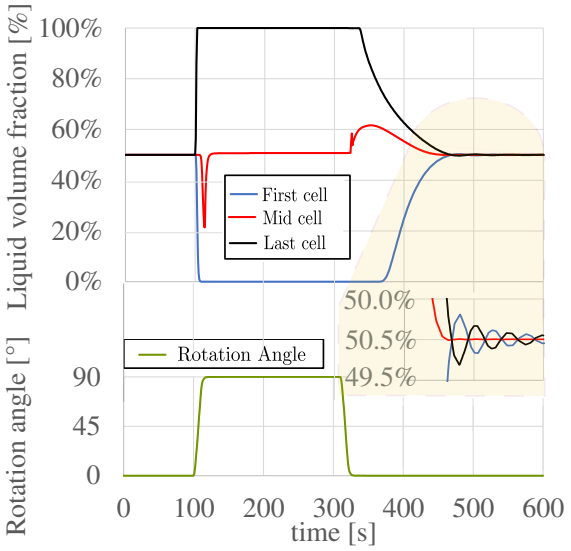

Figure 6. Resulted liquid volume fraction of the rotation test scenario.

test rigs was largely identical, the main difference being the use of a single or three parallel evaporators. In both cases, phase change material was considered as a heat load buffer at the evaporator. Figure 7 shows our test rig model within the Dymola graphical environment. The rising/-downcoming pipes and mass flow meter, as well as the evaporator and condenser models, are all based on the 6-equation flow models described above.

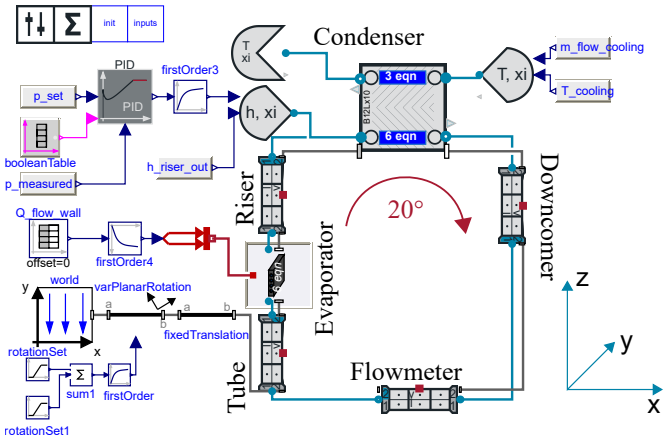

Figure 7. Diagram of measurement test rig model.

3.2.2 Heat Up and Shut Down Scenario

The first test scenario involves a sudden increase in heating power at the evaporator, followed by a sudden shutdown of the heater. Simulation results and measurement data are compared in Figure 8. The model is brought to steady state (corresponding the starting point of measured data) in several steps. Simulation is started with liquid in all the pipes and the cooling is on. After around 500 s, the heating is switched on. PID controller removes portion of flow until pressure reaches set point during operation. At around 2000 s the PID controller is disabled and the circuit is closed (self-regulating) and the system stabilizes (reaches steady state at 710 W).

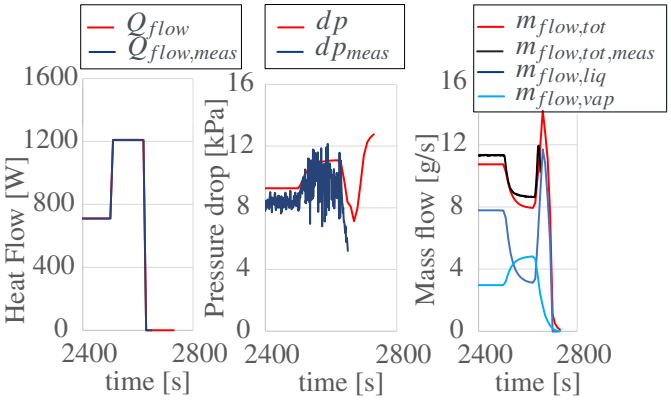

Figure 8. Heat flow (left), Pressure drop between evaporator inlet and condenser inlet (mid) and Mass flows of vapour and liquid (right), during heat up and shut down scenario.

During steady state operation at 710 W, the total mass flow through the system is around 11 g/s. Mass flow of liquid mass flow of vapour in evaporator is 8 g/s and 3 g/s respectively. During heat up to 1210 W, ε_{vap} increases. As a consequence mass flow of liquid drops to 3 g/s and mass flow of vapour increases to 5 g/s. After around 115 s (holding the new higher power level), a sudden power off (0 W) is introduced. This causes a decrease of vapour mass flow to 0 g/s and mass flow of liquid shortly increases (peaking after 30 s from shut down) as evaporator walls are still hot and pressure drop is high (caused by previous high mass flow of vapour). After reaching the peak (14 g/s), the mass flow of liquid also goes to zero, as there is no driving force (no heating). Figure 8 also shows the pressure drop between evaporator inlet and condenser outlet. There is higher pressure drop at higher heating power resulting from higher mass flow of vapour. Simulation results are in very good agreement with measured values. All steady state, heating ramp up and shut down processes were captured very well. Although measurements only provide information on the total mass flow, information on vapour/liquid mass flow can be derived (using total mass flow, pressure in the system and inlet/outlet temperature in evaporator) and energy and mass balance equations. The simulated results correspond very well to the derived values.

3.2.3 Rotation Scenario

The second scenario involves a rotation of the test rig running in steady state, reflecting a typical manoeuvre during a flight. The system is heated up by 850 W and steady state operation is achieved. At 2500 s a sudden (within 10 s) clockwise rotation by 20°around Y axis is introduced. After 300 s the system is turned back to normal position and reaches its initial steady state. Our model already captures the measured total mass flow drop during rotation qualitatively well. The quantitative deviation seems to be caused by the sudden change of spatial liquid/vapour distribution

and indicates that the currently simple models for friction and spatial distribution need further elaboration.

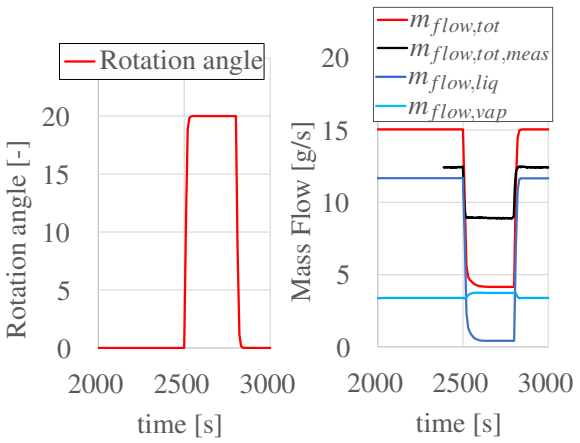

Figure 9. Rotation angle (left) and Mass flows of vapour and liquid (right) during the rotation scenario.

4 Summary & Outlook

In this paper we present a numerically robust implementation of detailed two phase model based on the six-equation approach. To achieve this we introduce an alternative set of extensive state variables from which specific quantities static pressure and volume fractions of the vapour and liquid phase can be computed algebraically. The applicability of the model is demonstrated in several testers. Currently the model is further developed to feature more detailed models for friction, spatial distribution and heat transfer, e.g. (Hoppe, Gottelt, and Wischhusen 2017). It is also straightforward to extend the model to feature multi-component media. The model has potential application in several areas of engineering, from aerospace, automotive and naval systems design to power plants and process technologies. Typical industrial systems with two phase heat exchangers such as evaporators, boilers, steam generators and condensers would be typical example of application, especially when it comes to non-standard transient operation scenarios, e.g. start up/shut down, heat up/cool down, filling or draining of the system under investigation.

Acknowledgements

The authors would like to thank the NAKULEK research team as well as E. Makhova, T. Tumforde and J. Eiden from XRG for support and discussions. This work has been carried out within the NAKULEK research project, funded by the German Federal Ministry for Economic Affairs and Energy (grant number 20Q1519B).

Supported by:
Federal Ministry for Economic Affairs and Energy
on the basis of a decision by the German Bundestag

Moreover we thank the anonymous referees for their valuable remarks.

References

Albertsen, Björn and Gerhard Schmitz (2019). *NAKULEK - Entwurf, Bau und Erprobung eines PCM-Kühlplatten Verbunds für eine Naturumlaufkuehlung von Flugzeugsystemen : Abschlussbericht*. German. Technical University Hamburg, Germany. DOI: https://doi.org/10.2314/KXP:1753985420. (Visited on 2021-04-19).

Bauer, O. (1999). "Modeling of two-Phase Flows with Modelica". MA thesis. Department of Automatic Control, Lund Institute of Technology, Sweden.

Bonilla, J. et al. (2012). "Object-Oriented Library of Switching Moving Boundary Modelsfor Two-phase Flow Evaporators and Condensers". In: *Proceedings of the 9th International Modelica Conference*, pp. 71–80.

Brennen, Christopher E. (2005). *Fundamentals of Multiphase Flows*. Cambridge University Press. ISBN: 0521 848040.

Brunnemann, Johannes (2020). *NAKULEK - Naturumlaufkühlung für Leistungselektronik : Schlussbericht*. German. XRG Simulation GmbH. DOI: https://doi.org/10.2314/KXP:1755577478. (Visited on 2021-04-19).

ClaRa Development Team, ed. (2021). *ClaRa*. Version 1.6.0. URL: https://claralib.com/.

Francke, H. (2014). "Thermo-hydraulic model of the two-phase flow in the brine circuit of a geothermal power plant". PhD thesis. Technical University Berlin,Germany.

Ghiaasiaan, S. Mostafa (2008). *Two-Phase Flow, Boiling and-Condensation. IN CONVENTIONAL ANDMINIATURE SYSTEMS*. Cambridge University Press.

Hänninen, Markku and Jukka Ylijoki (2008). *The one-dimensional separate two-phase flow model of APROS*. English. VTT Tiedotteita - Meddelanden - Research Notes 2443. VTT Technical Research Centre of Finland. 65 pp. ISBN: 978-951-38-7225-0. URL: http://www.vtt.fi/inf/pdf/tiedotteet/2008/T2443.pdf (visited on 2021-04-19).

Hoppe, T., F. Gottelt, and S. Wischhusen (2017). "Extended Modelica Model for Heat Transfer of Two-Phase Flows in Pipes Considering Various Flow Patterns". In: *Proceedings of the 12th International Modelica Conference, Prague, Czech Republic, May 15-17, 2017*. Linköping University Electronic Press, Linköpings universitet, pp. 467–476.

Jensen, J.M. and H. Tummescheit (2002). "Moving Boundary Models for Dynamic Simulations of Two-Phase Flows". In: *Proceedings of the 2nd International Modelica Conference*, pp. 235–244.

Quaium, Farid and Holger Kuhn (2020). *NAKULEK - Naturumlaufkuehlung für Leistungselektronik : Abschlussbericht*. German. ZAL Center of Applied Aeronautical Research, Hamburg, Germany. DOI: https://doi.org/10.2314/KXP:1747878758. (Visited on 2021-04-19).

Skogestad, S. (2009). *Chemical and Process Engineering*. CRC Press. Chap. 11.

Sokolichin, Alexander (2003). "Mathematical modeling and numerical simulation of gas-liquid bubbly flows". Habilitation Thesis, University of Stuttgart, Germany.

VERSTEEG, H. K. and W. MALALASEKERA (1995). *An introduction to computational fluid dynamics. The finite volume method*. Longman Scientific & Technical, pp. 62–67.

Whalley, P. B. (1987). *Boiling, Condensation, and Gas-Liquid Flow*. Clarendon Press, Oxford.